공학석사 학위논문

Conduction mechanism change according to barrier height of oxide hetero-interface diode

산화물 적층 계면의 박막 다이오드의 장벽 높이에 따른 전도 메커니즘의 변화

2017 년 8 월

서울대학교 대학원

융합과학부 나노융합전공

남 부 일

Conduction mechanism change according to barrier height of oxide hetero-interface diode

지도교수 김 연 상

이 논문을 공학석사 학위논문으로 제출함

2017 년 8 월

서울대학교 대학원
융합과학부 나노융합전공
남 부 일

남부일의 석사학위논문을 인준함
2017 년 7 월

위 원 장 송 윤 규 (인)

부 위 원 장 김 연 상 (인)

위 원 이 강 원 (인)

Abstract

Conduction mechanism change according to barrier height of oxide hetero-interface diode

Bu-il Nam

Program in Nano Science and Technology

Department of Transdisciplinary Studies

The Graduate School of

Seoul National University

An effective and facile strategy is proposed to demonstrate an engineered oxide hetero-interface of a thin film diode with a high current density and low operating voltage. The electrical characteristics of an oxide hetero-interface thin film diode are governed by two theoretical models: the space charge-limited current (SCLC) model and the Fowler-Nordheim (F-N) tunneling model. Interestingly, the dominant mechanism strongly depends on the insulator thickness, and the mechanism shift occurs at a critical thickness. This phenomenon is seen by a

decrease in the barrier height at the insulator / semiconductor interface as the thickness of the insulator increases. This paper shows that the barrier heights of oxide hetero-interface thin film diodes can be changed by simple engineering of the insulator layer thickness. These oxide hetero-interface diodes have great potential for low-powered transparent nanoscale applications.

……

Keywords : oxide hetero interface, thin film diode, barrier height, mechanism shift, interface dipole

***Student Number* : 2015-26090**

Contents

List of tables

List of figures

1. Introduction

1.1 Current Trend in Oxide Thin Film Diodes

During the past half century, research on thin film diodes and their applications have greatly contributed to the development of the modern IT industry. [1-3] Recently, in the display industry, because transparent electronics have emerged as the next-generation technology, various p-n junction, Schottky junction and metal-insulator-metal (MIM) diodes have been investigated for transparent diodes.[4-6] In particular, oxide semiconductor materials have received much attention as major materials for transparent diodes because of their excellent properties which include high charge carrier mobility, great electrical conductivity, good optical transparency and easy control of thin-film fabrication.[7]

However, despite their many merits, there are big challenges to developing transparent thin film diodes. In the case of p-n junction diodes, most of the oxide semiconductor materials are inherently n-type semiconductors due to their intrinsic oxygen vacancies. In detail, substitution and interstitial impurities increase the donation of electrons to the conduction band and intrinsically provide charge carriers for n-type semiconductors.[8,9] In addition, conventional p-type oxide

semiconductors have poor electrical properties such as a very low carrier mobility due to a large hole effective mass. For these reasons, the development of the p-type oxide semiconductor and commercialization of transparent p-n diodes are very difficult.[10,11] Meanwhile, in the case of Schottky junction diodes, oxide Schottky diodes have been widely developed because they are relatively simple in structure and can be fabricated only with n-type semi-conductors. However, their applications are considerably limited due to their poor reverse leakage current and low rectifying current ratio.[12,13]

1.2 Introduction of MEEM Diodes

Recently, oxide hetero-interface thin film diodes were newly reported to overcome the disadvantages of these conventional diodes. This diode (Figure 1) is called the MEEM diode: MEEM, metal-ETO-EIO-metal; ETO, electron-transporting oxide, the oxide insulator, and EIO, electron-injecting oxide, the oxide semiconductor. The diode has a thin film with an oxide hetero-structure consisting of an oxide insulator and oxide semiconductor junction. When transparent metals are used for both electrodes in oxide hetero-interface thin film diodes, they can be transparent diodes.[14,15] Surprisingly, unlike conventional diodes, MEEM diodes have a unique characteristic: considerable electric currents flow through a relatively thick insulator.[14,15] In addition, MEEM diodes have great potential for nanotechnology applications because they have various advantages including a simple structure, easy process control, low leakage current, high rectifying current ratio, zero volt switching and transparency. However, there are no specific studies yet that accurately describe the electrical flows and conduction mechanism; therefore, it is essential to take the next step to clarify the new electrical behavior, especially based on physical theory. This will help find a way to compensate for the weaknesses of conventional MEEM diodes such as low forward current characteristics at low voltages and challenge many applications.

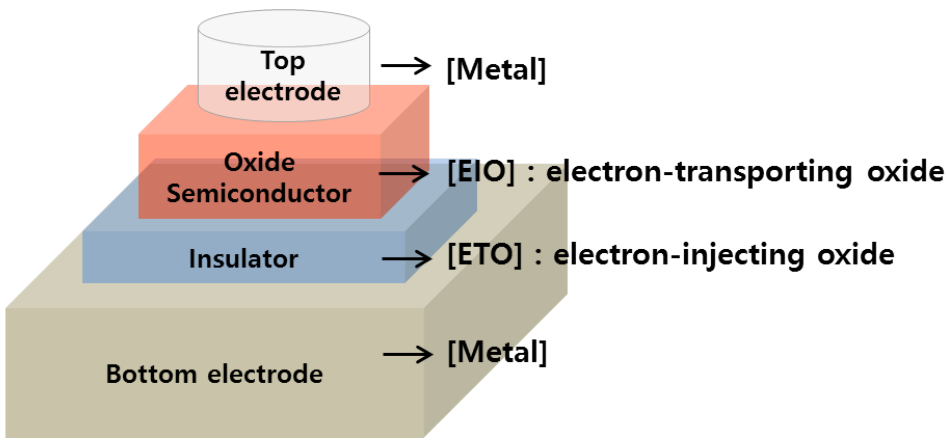

Figure 1. A schematic stucture of the oxide thin film diode with Metal electrode / EIO / ETO / Metal electrode (MEEM).

1.3 Barrier Heights of MEEM Diodes

Herein, this study shows for the first time that the barrier heights of the ETO / EIO interface in an oxide hetero-interface diode, a MEEM diode, vary with the thickness of the ETO insulating layer (t_{ETO}). Additionally, due to these variations in the barrier height, the conduction mechanisms change at a certain t_{ETO}. More specifically, when the t_{ETO} is reduced from 50 nm to 3 nm, the field emission behavior in the forward bias changes from the space charge-limited current (SCLC) model to the Fowler-Nordheim (F-N) tunneling model.[16,17] In addition, the variation in the barrier height can be calculated by a significant current difference between the MIM and MEEM structures with very thin insulators because both structures follow the same F-N tunneling model. Thus, it is easily seen that barrier height variations occur at the interface between the semiconductor and insulator of the MEEM diode resulting in a large rectifying current density of more 10^7 times than that of the MIM device. Consequently, a simple engineering approach to barrier height of MEEM diodes has been developed by controlling the t_{ETO}.

This approach enables the engineering of MEEM diodes with an excellent forward current density (0.16 A/cm^2) and rectifying ratio (2×10^7) at a low operating voltage (±3 V).

2. Experimental Process

2.1 Fabrication and Measurement of Devices

Fabrication of MEEM didoes

MEEM diodes (Figure 2) were fabricated on cleaned 1 inch x 1 inch highly B-doped Si substrates. These substrates were washed sequentially with detergent, double-distilled water, acetone, and isopropyl alcohol. Y_2O_3 films with thicknesses from 3nm to 50 nm were grown by atomic layer deposition (ALD) with $Y(iPrCp)_2(N\text{-}iPr\text{-}amd)$ precursor and O_3 counter-reactant in custom-designed ALD chamber at substrate temperature of 200 °C. ZnO thin films with thicknesses of 20nm were deposited on the Y_2O_3 / P^{++} Si substrate by radio frequency (RF) magnetron sputtering which was in RF power of 90 W with a gas flow ratio of Ar: O_2 = 25 sccm: 0 sccm under a working pressure of 10 mTorr at room temperature. These samples were treated by rapid thermal annealing (RTA) treatments (atmospheric pressure, 350 °C, 90 seconds) to achieve improved electrical current characteristics. And then, aluminum circle electrodes were deposited by thermal evaporation at a working pressure of 10^{-6} mTorr. The electrodes were designed with a radius of 250 μm and a height of 50 nm.

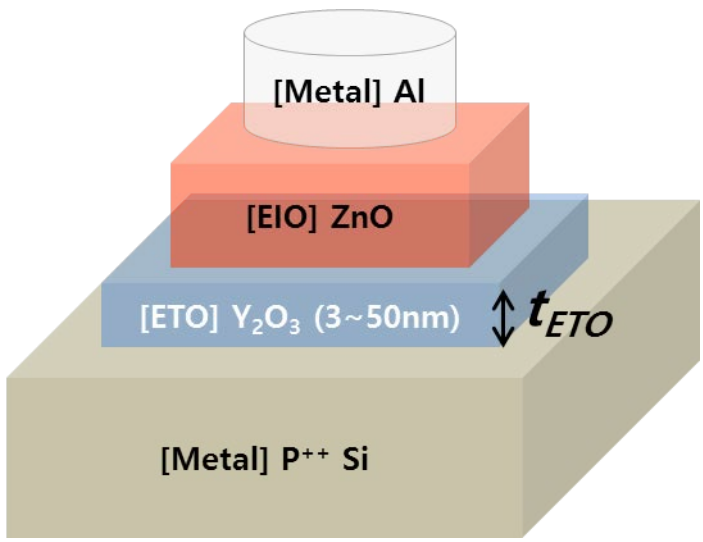

Figure 2. A schematic stucture of the MEEM diode with aluminum / ZnO / Y_2O_3 / P^{++} Si structure.

Fabrication of the MIM devices

MIM devices (Figure 3) were fabricated in the same process as the MEEM diodes except for ZnO RF sputtering. The MIM devices were fabricated on cleaned 1 inch x 1 inch highly B-doped Si substrates. These substrates were washed sequentially with detergent, double-distilled water, acetone, and isopropyl alcohol. Y_2O_3 films with thicknesses from 3nm to 50 nm were grown by atomic layer deposition (ALD) with $Y(iPrCp)_2(N\text{-}iPr\text{-}amd)$ precursor and O_3 counter-reactant in custom-designed ALD chamber at substrate temperature of 200 °C. And then, aluminum circle electrodes were deposited by thermal evaporation at a working pressure of 10^{-6} mTorr. The electrodes were designed with a radius of 250 μm and a height of 50 nm.

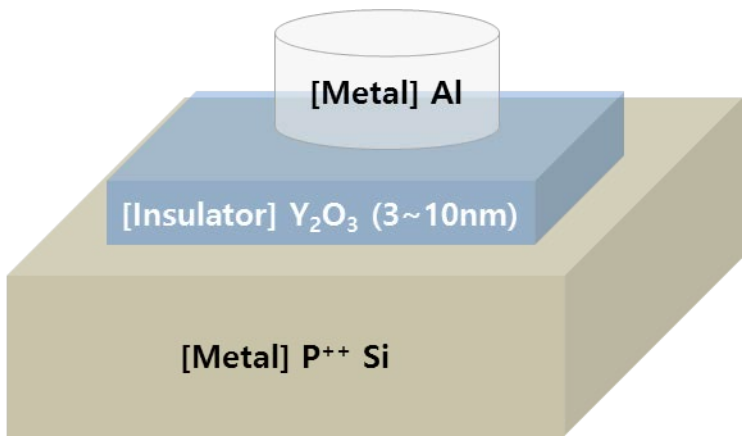

Figure 3. A schematic stucture of the MIM diode with aluminum / Y_2O_3 / P^{++} Si structure.

Characteristic measurement of devices

Electrical characteristics of all diodes were measured in a dark and atmosphere condition using Agilent Technologies 4155B semiconductor parameter analyzer.

3. Results and Discussion

3.1 Mechanism Shift According to Insulator Thickness

To study the electrical characteristics at the ETO / EIO interface in an oxide hetero-interface diode, or a MEEM diode, Yttrium oxide (Y_2O_3) and ZnO, for which the former is a high-k material with excellent insulating properties, were prepared for the ETO and EIO layer, respectively.[18] The MEEM structures (Figure 2) were fabricated to confirm the unidirectional electrical currents, which were previously reported.[14,15] The ETO layers were deposited at various thicknesses from 3 to 50 nm shown in Figure 2. Remarkably, a new phenomenon for the t_{ETO} in the MEEM diode was found, that is, the forward currents increase exponentially as the t_{ETO} becomes thinner than 10 nm, and the current conduction mechanisms are clearly divided according to the t_{ETO}.

Figure 4 shows the forward current density of the MEEM diode according to the t_{ETO}. These data represent the current density extracted from all the diodes with varying thicknesses at a forward bias 3V. In the plot of log J versus t_{ETO}, all the data are separated into two distinct thickness regions. It was identified that the current conduction mechanisms of the 3 to 10 nm region and the 20 to 50 nm region are

different. With the measured data, sub-10 nm t_{ETO} were fitted with the F-N tunneling model curve, and over-20 nm t_{ETO} were fitted with the SCLC model curve. Thus, it is reasonable to deduce that the current conduction mechanism shift occurs at a particular t_{ETO}.

For more detailed evidence of the thickness dependence between the two mechanisms, the current density data at each t_{ETO} were fitted to both mechanism model plots. The following current density equations of these two theories were used in this work. First, according to the SCLC theory, the current density J is as follows:

$$J_{SCLC} = \sigma_0 \left[\frac{\varepsilon_0 \varepsilon_i l \sin(\pi/l) l^4}{q(l+1)B_c(2\alpha)^3}\right]^l \left(\frac{2l+1}{l+1}\right)^{l+1} \left(\frac{1}{d}\right)^{2l+1} V^{l+1} \quad (1)$$

$$log(J) \propto log(V) \quad (2)$$

where σ_0 is the conductivity prefactor, B_c is the critical number for percolation onset, α is the effective overlap parameter for the electron-hopping process, ε_i is the dielectric constant of the material, ε_0 is the permittivity of the free space, q is the elementary charge, d is the thickness of the material, and $\ell = T_0/T$, where T_0 is the trap-characteristic temperature.[14-16] Equation (2) is the simplified version of Equation (1). This shows that if SCLC plot (*log V* versus *log J*) are linearly matched, they follow the SCLC theory (Induction of the SCLC plot, Supplementary). Second, also according to the F-N theory, the field emission current density J is as follows:

$$J_{FN} = \frac{a(\beta V)^2 A}{\emptyset_B d^2} \exp\left(-\frac{bd\emptyset_B{}^{3/2}}{\beta V}\right) \quad (3)$$

$$ln\left(\frac{J}{V^2}\right) \propto -\frac{1}{V} \quad (4)$$

where d is the t_{ETO}, β is the field enhancement factor at the emitter surface, A is the area of emission, Φ_B is the barrier height at the injection interface, and a and b are geometric constants. [17,19] Equation (4) is the simplified version of Equation (3). This shows that if the F-N plot ($ln\ J\ /\ V^2$ versus $1\ /\ V$) are linearly matched, they follow the F-N tunneling mechanism (see section 3.2 Induction of the F-N plot). Figure 5 shows further verifications of the current conduction mechanism for each thickness using these equations. The curves of the SCLC plot in Figure 5(a) show that current densities of 20, 25, and 50 nm t_{ETO} linearly match with SCLC model. The curves of F-N plot in Figure 5(b) show that current densities of various t_{ETO} (3, 5, 7 and 10 nm) linearly match with the F-N tunneling model. The R-squared (R^2) of the data is over 0.99 (Table 1), which indicates that these data accurately confirm the SCLC or F-N tunneling mechanism. The value of the determinant factor in statistics, R^2, which is a measure of how well an estimated linear model is appropriate for a given data set, is close to 1, which means that the experimental data fit exactly with the assumed model.[20] These data clearly show that MEEM diodes operate with two types of mechanisms depending on the t_{ETO}.

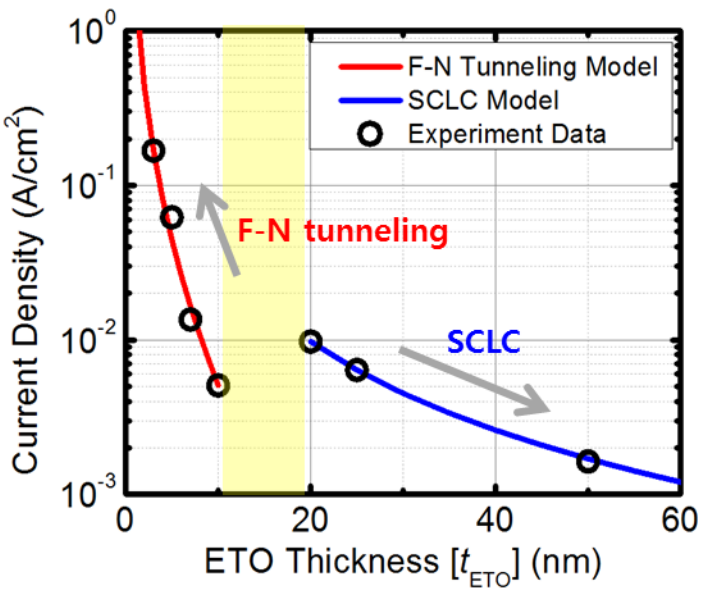

Figure 4. The current densities depending on the t_{ETO} at 3 V forward bias. The measured data (black circle), the calculated F-N tunneling model (red line) and the calculated SCLC model (blue line).

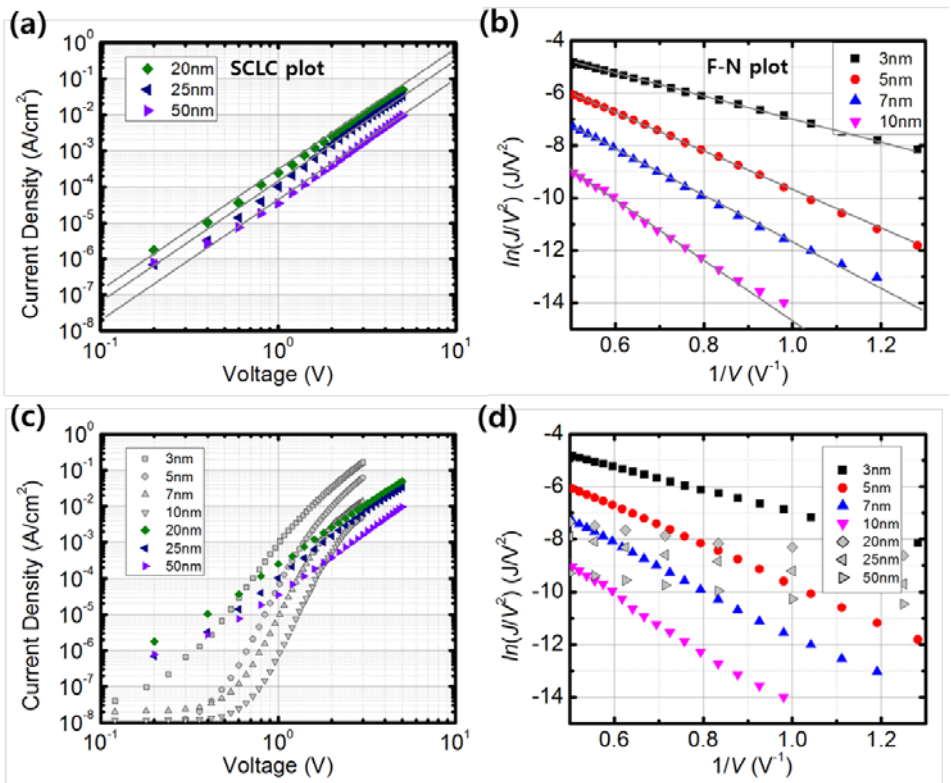

Figure 5. The characteristics of current densities at t_{ETO} from 3nm to 50nm. (a) The relatively thick insulator diodes (t_{ETO} = 20~50 nm) are linearly fitted in the SCLC plot, which can be estimated with the SCLC mechanism. (b) The ultra-thin insulator diodes (t_{ETO} = 3~10 nm) are linearly fitted in the F-N plot, which can be estimated with the F-N tunneling mechanism. (c,d) The characteristics of diodes in all t_{ETO} are divided into two parts at about 15 nm.

t_{ETO}	*3nm*	*5nm*	*7nm*	*10nm*	*20nm*	*25nm*	*50nm*
SCLC model	0.9897	0.9253	0.8717	0.8192	**0.9987**	**0.9965**	**0.9908**
F-N tunneling model	**0.9988**	**0.9982**	**0.9978**	**0.9968**	0.8422	0.9299	0.9188

Table 1. The value of determinant factor in statistics. R^2 value in Figure 5. The closer to 1, the more conformity with the estimated model. (Only 0.99 or more are blue letters)

3.2 Induction of Plots

Induction of the SCLC plot.

According to SCLC theory, the current density is described as follows[1-3].

$$J_{SCLC} = \sigma_0 \left\{\frac{\varepsilon_0 \varepsilon_i l \sin(\pi/l) l^4}{q(l+1)B_c(2\alpha)^3}\right\}^l \left(\frac{2l+1}{l+1}\right)^{l+1} \left(\frac{1}{d}\right)^{2l+1} V^{l+1} \quad , \qquad (5)$$

σ_0 is the conductivity prefactor, B_c is the critical number for percolation onset, α is the effective overlap parameter for the electron-hopping process, ε_i is the dielectric constant of the material, ε_0 is the permittivity of the free space, q is the elementary charge, d is the thickness of the material, and $\ell = T_0/T$, where T_0 is the trap-characteristic temperature.[1-3] Another way to write SCLC equations that can be easily visualized and quantified in SCLC plots take the common logarithm on both sides.

$$log(J_{SCLC}) = log\left[\sigma_0 \left\{\frac{\varepsilon_0 \varepsilon_i l \sin(\pi/l) l^4}{q(l+1)B_c(2\alpha)^3}\right\}^l \left(\frac{2l+1}{l+1}\right)^{l+1} \left(\frac{1}{d}\right)^{2l+1}\right] + (l+1)log(V) \quad , \qquad (6)$$

The relation between voltage and current density is abbreviated as follows.

$$log(J_{SCLC}) \propto log(V) \quad , \qquad (7)$$

Therefore, the SCLC curve should be linear with a positive slope of the log(J) versus log (V) plot.

Induction of the F-N plot.

According to F-N tunneling theory, the current density is described as follows.

$$J_{FN} = \frac{a(\beta V)^2 A}{\emptyset_B d^2} \exp\left(-\frac{bd\emptyset_B{}^{3/2}}{\beta V}\right) \quad , \qquad (8)$$

where d is the t_{ETO}, β is the field enhancement factor at the emitter surface, A is the area of emission, Φ_B is the barrier height at the injection interface, a and b are geometric constants.[4,5] Another way to write F-N tunneling equations that can be easily visualized and quantified in F-N plots take the natural logarithm on both sides.

$$ln\left(\frac{J_{FN}}{V^2}\right) = ln\ \frac{a\beta^2 A}{\emptyset_B d^2} - \frac{bd\emptyset_B{}^{3/2}}{\beta}\left(\frac{1}{V}\right) \quad , \qquad (9)$$

The relation between voltage and current density is abbreviated as follows.

$$ln\left(\frac{J}{V^2}\right) \propto -\frac{1}{V} \quad , \qquad (10)$$

Therefore, the F-N tunneling curve should be linear with a negative slope of the $ln\ J / V^2$ versus $1 / V$ plot.

3.3 Variation of Barrier Height Depending on Existence of Semiconductors

When the t_{ETO} is sub-10 nm, it follows the F-N tunneling mechanism, which is a commonly known mechanism for MIM devices.[21] Therefore, if both devices, MIM and MEEM devices, have the same mechanism with an ultra-thin insulating layer, it means that they can be represented by the same equation. Thus, various parameters for MEEM diodes can be obtained from the characteristics of conventional MIM devices. The most important of these parameters is the barrier height of the MEEM diode, which is a critical parameter for the generation of electron flow in F-N tunneling conduction. The equation (Equation (11)) for obtaining the barrier height of a MEEM diode ($\Phi_{B(MEEM)}$) from the barrier height of a MIM device ($\Phi_{B(MIM)}$) was derived using Equation (3) (The barrier height equation of the MEEM diode, Supplementary).

$$\emptyset_{B(MEEM)} = \emptyset_{B(MIM)} \left(\frac{m_{(MEEM)}}{m_{(MIM)}}\right)^{2/3} \quad (11)$$

Here, m is the slope of the F-N plot.[19] For these reasons, two devices, as shown in Figure 6(a), were fabricated. One was a MEEM Diode and the other a MIM device both with t_{ETO} of 7 nm. In Figure 6(a), the forward current density (0.07 A/cm^2) at 3V of the MEEM device is 10^7 times higher than that (6.8×10^{-9} A/cm^2) of the MIM device. Additionally, in the SCLC plot graph (Figure 6(a)), it was found that there is a unidirectional current characteristic only in the MEEM structure, while in the

graph of the F-N plot (Figure 6(b)), it was confirmed that for the conduction mechanisms of both structures, the MIM and MEEM devices, F-N tunneling was dominant. Therefore, it was verified that the MIM and MEEM devices with a 7nm thick Y_2O_3 insulator can use Equation (11). Because the barrier height of Y_2O_3 / Al was reported as 2.5eV, [22] the barrier height of Y_2O_3 / ZnO was calculated with Equation (11) to be $\Phi_{B(MEEM)}$ = 1.1eV, which are expressed using band diagrams in Figure 9(a,b).

The bands are aligned based on the vacuum level. In general, the work function of Al and ZnO is almost equal to 4.2 eV. Therefore, $\Phi_{B(MIM)}$ and $\Phi_{B(MEEM)}$ should theoretically be approximately equal to 2.5 eV; however, the experimental results show that the two barrier heights are 2.5 eV and 1.1 eV with a difference of 1.4 eV. The cause of this difference can be predicted to be from various phenomena as follows: interface dipoles at high-k/SiO2,[23-25] interface dipoles at metal/oxide/organic,[26,27] polarization dipoles found in ferroelectrics,[28,29] and polarization dipoles by the strain-induced electric field.[30,31] Their common feature is the barrier height variations caused by the dipole moments, which are induced by each effect in the junction structure of other materials. These effects are explained by dipole formation caused by the areal density difference of the oxygen atoms,[23-25] dipoles induced in charge transfer by chemisorption of the organic layer,[26,27] ionic built-in potential by electron gas and dipoles induced in piezoelectric strain.[28-31] However, because Y_2O_3 is not a ferroelectric or crystal piezoelectric material, it

cannot be an ionic potential and a polarity dipole. In addition, because ZnO is an inorganic material, it is certainly not an organic layer chemisorption dipole. Therefore, it can be assumed that the dipole moments can be formed by a change in electron distribution or ion arrangement due to the density difference of the oxygen atoms. According to this logic, as the normalized oxygen areal density becomes smaller than 1, the barrier height difference becomes larger.[23-25] Calculating the normalized oxygen areal density of Y_2O_3 and ZnO, when Y_2O_3 is 1, ZnO is 0.93, which is less than 1 (Figure 8, Table 2). In addition, ZnO sputtering is known to cause many oxygen defects.[32,33] When the oxygen deficiency is about 10%, the normalized oxygen areal density reaches 0.84, and the barrier height difference becomes larger (Figure 8, Table 2). This hypothesis could be valid as the operating principle of MEEM diodes; however, an in-depth study is needed to prove it clearly. It was verified by the formula that the barrier height of a MEEM diode with an ultra-thin film insulator is reduced. These barrier height variations are presumed to be caused by the interface dipole created by the difference in oxygen density per unit area of the materials at both ends of the junction shown in Figure 7. Figure 9(b) shows a band diagram in which these dipoles reduce the barrier height.

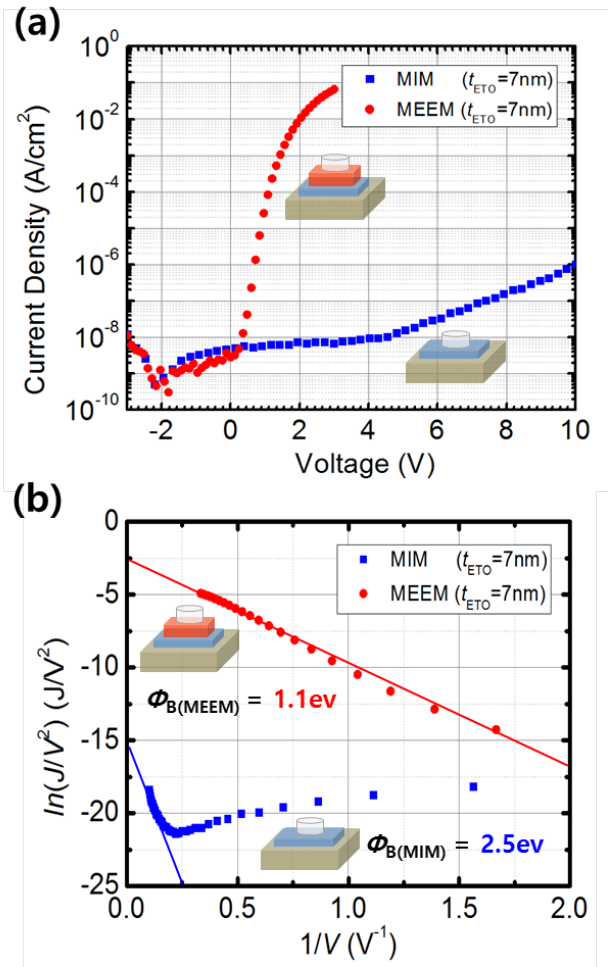

Figure 6. (a) The J-V curve comparison of the MIM and the MEEM structure diode (t_{ETO} =7nm). (b) Both diode current densities are linearly fitted in the 1/V-ln (I/V2) scale, so both can be seen as the same F-N tunneling mechanism. The barrier height of MIM is 2.5 eV, and the barrier height of MEEM can be calculated as 1.1 eV by Equation (11).

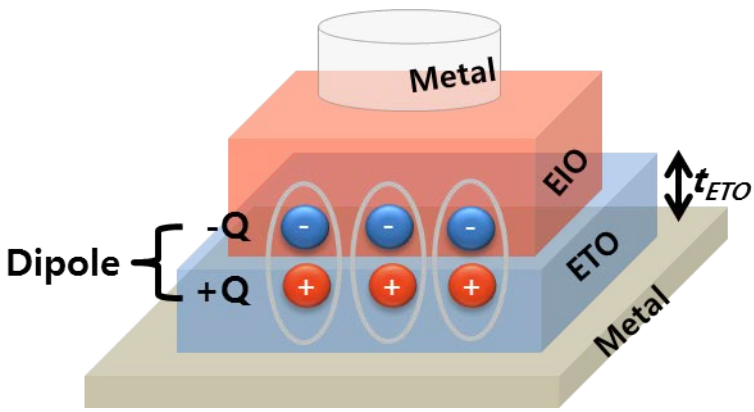

Figure 7. A schematic of the MEEM structure. The ETO / EIO interface might have dipole moments.

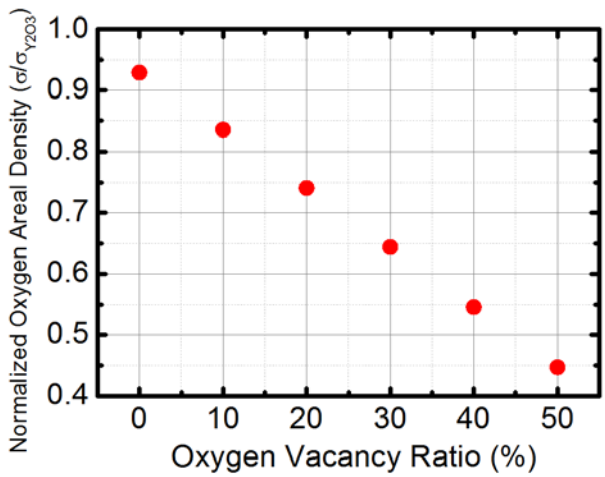

Figure 8. The normalized oxygen areal density versus the oxygen vacancy ratio of ZnO. At the junction of Y_2O_3 and ZnO, the more oxygen vacancy ratio of ZnO layer is, the lower the normalized oxygen areal density. The farther the value of the normalized oxygen areal density is from 1, the larger the interface dipole moments. The calculated values are listed in Table 3.

Oxygen vacancy ratio	0%	0%	10%	20%	30%	40%	50%
Chemical formula	Y_2O_3	ZnO	$ZnO_{0.9}$	$ZnO_{0.8}$	$ZnO_{0.7}$	$ZnO_{0.6}$	$ZnO_{0.5}$
Density ρ[g/cm3]	4.8	5.6	5.6	5.6	5.6	5.6	5.6
Unit structure	$Y_{2/3}O$	Zn_1O	$Zn_{1/0.9}O$	$Zn_{1/0.8}O$	$Zn_{1/0.7}O$	$Zn_{1/0.6}O$	$Zn_{1/0.5}O$
Mu[g/mol]	75.3	81.4	81.4	81.4	81.4	81.4	81.4
Vu[Å3]	26	29	34	41	50	65	87
σ/σ_{Y2O3}	1	0.93	0.84	0.74	0.64	0.55	0.45

Table 2. The normalized oxygen areal density. The values for the normalized oxygen areal density shown in Figure 8 are listed.

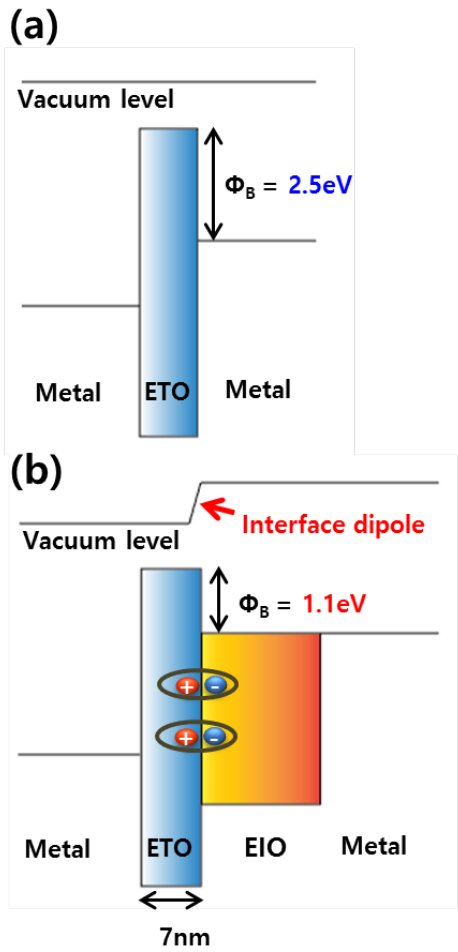

Figure 9. Band alignments as inferred from experimental data. (a) Band alignment of metal / ETO / metal structures based on vacuum level after contact. (b) The band alignment across the metal / ETO / EIO / metal structure in ETO of sub-10nm thickness.

3.4 Induction of The Barrier Height Equation

In Equation S5, the parameter of 1 / *V* is the slope of the F-N plot. Thus, the slope *m* in the F-N plot is given by

$$m = \left(\frac{bd\emptyset_B{}^{3/2}}{\beta}\right) \quad , \tag{12}$$

Assuming that the change of the factors other than the barrier heights between the MEEM and the MIM structure is negligibly small, the slope of the F-N plot of the MEEM and MIM structure is as follows.

$$m_{(MEEM)} = \left(\frac{bd\emptyset_{B(MEEM)}{}^{3/2}}{\beta}\right) \quad , \tag{13}$$

$$m_{(MIM)} = \left(\frac{bd\emptyset_{B(MIM)}{}^{3/2}}{\beta}\right) \quad , \tag{14}$$

If Equation S8 and Equation S9 are combined, the following equation can be obtained.

$$\emptyset_{B(MEEM)} = \emptyset_{B(MIM)} \left(\frac{m_{(MEEM)}}{m_{(MIM)}}\right)^{2/3} \quad , \tag{15}$$

By using this equation, the barrier height of the MEEM diode can be calculated.

3.5 Variation of Barrier Height Depending on Insulator thickness

Meanwhile, when the t_{ETO} of the MEEM diodes is more than 20 nm, the threshold voltage becomes 0 V, and a unidirectional current is generated even at a very small voltage. It can be inferred that the barrier height between ETO and EIO is very small or zero. Current densities above 20 nm t_{ETO} are higher than those at a t_{ETO} below 10 nm at very low voltages (about 0.2 V). Here, a critical thickness of ETO (t_{ETO}^{cr}) to account for this phenomenon was proposed. It can be easily understood by the band diagrams in Figure 10(a,b). These show band alignments of the MEEM diodes around t_{ETO}^{cr}. When t_{ETO} is below t_{ETO}^{cr}, the barrier height is greater than zero, which forms a certain barrier, and when t_{ETO} is above t_{ETO}^{cr}, the barrier height becomes zero, which forms an ohmic-like contact. This band diagram shows that as the t_{ETO} increases to a certain point, the barrier height decreases. Conversely, the generation of dipoles continues to increase until the t_{ETO} becomes t_{ETO}^{cr}. This hypothesis is supported by the experimental results obtained by observing the change in the barrier height according to t_{ETO}. Figure 11(a) shows the barrier height of the ETO / EIO interface according to t_{ETO}. As seen in Table 3, increasing the t_{ETO} from 3 nm to 10 nm reduces the barrier height from 1.3 eV to 0.9 eV. This barrier height was calculated by Equation (11). This result shows that the barrier height becomes smaller as t_{ETO} becomes thicker, and t_{ETO}^{cr} is expected to be in a range from 15 nm to 20 nm (Figure 11(b)).

Figure 12 show the flows of the electrical current generated when a positive bias is applied. Figure 12(a) shows the electrical current flows in the case when the t_{ETO} is thinner than the t_{ETO}^{cr}, and many electrons passed from the metal cathode to the EIO encounter the certain barrier height in the ETO interface and penetrate the ETO through quantum tunneling by the applied electric fields. Figure 12(b) shows the electrical current flows in the case when the t_{ETO} is thicker than the t_{ETO}^{cr}, and many electrons passed from the metal cathode to the EIO smoothly pass to ETO because Φ_B = 0 eV, and the space charges are filled in the ETO and overflow to the metal anode. At this point, the current flows follow the SCLC conduction model. The fact that the barrier height of devices following the SCLC mechanism is close to zero has been shown in previous studies. [16,34,35]

The changes in the barrier height according to the t_{ETO} were empirically confirmed in this experiment; however, the theory is not exactly known. However, it can be estimated from the following previous reports: The dipole formation varies depending on the thickness in the high-k / SiO2 layer experiment, and the dipole moments are changed by the atomic concentration change depending on the distance from the surface in the HfLaOx / SiO2 structure.[24,36] Additionally, as the thickness of the ferroelectric material becomes thicker, the potential difference between both ends is increased by the induced polarization, and the barrier height is lowered accordingly.[28] The common points of these reports are that thicknesses above the critical thickness are essential for maximizing the interface dipoles or

induced polarizations. Therefore, t_{ETO}^{cr} is required to obtain the maximum dipole moment on the ETO / EIO surface in MEEM diodes, and in the case when t_{ETO} is over the value of the t_{ETO}^{cr}, a sufficient dipole formation is generated, and the barrier height reaches zero. At this point, the current flow mechanism switches from the F-N tunneling to the SCLC conduction model.

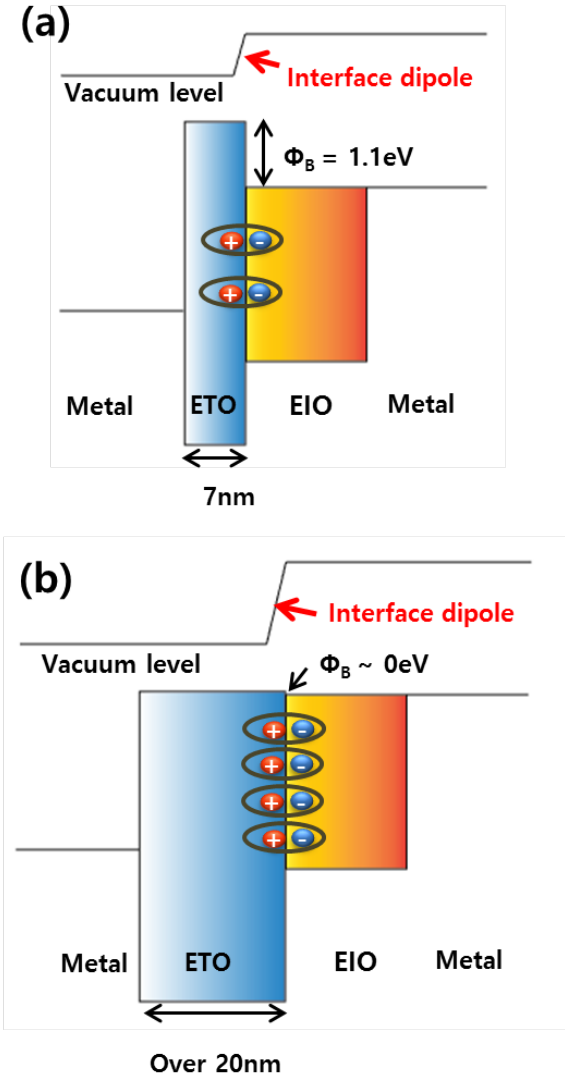

Figure 10. (a) The band alignment across the metal / ETO / EIO / metal structure in ETO of sub-10nm thickness. (b) The band alignment in ETO of over-20nm thickness. Sufficient t_{ETO} is required to obtain the maximum dipole moments.

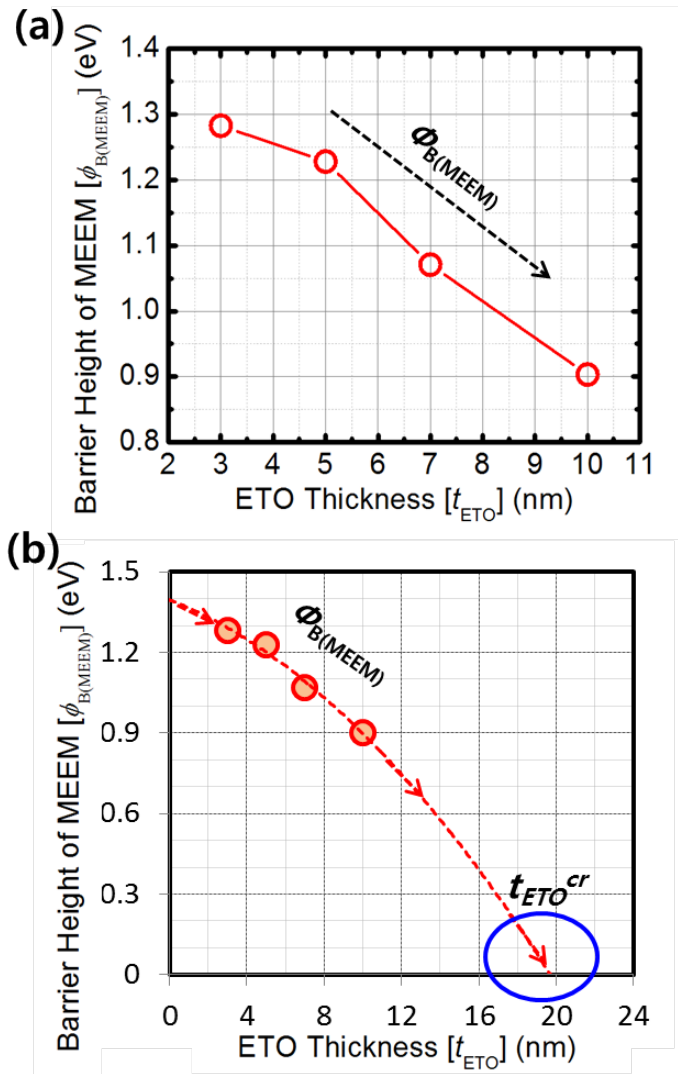

Figure 11. (a) The barrier heights of MEEM diodes according to t_{ETO}. (b) The thickness of the ETO where the trend line becomes zero barrier height can be estimated as t_{ETO}^{cr}.

t_{ETO} [nm]	m(slope of F-N plot)		$\Phi_{B(MEEM)}$ [eV]
	MIM	MEEM	
3 nm	-11.4	-4.2	1.28 eV
5 nm	-21.5	-7.2	1.23 eV
7nm	-30.6	-8.7	1.07 eV
10nm	-50.1	-10.9	0.90 eV

Table 3. F-N slopes of the MIM and MEEM structure for each t_{ETO}, and the calculated barrier height

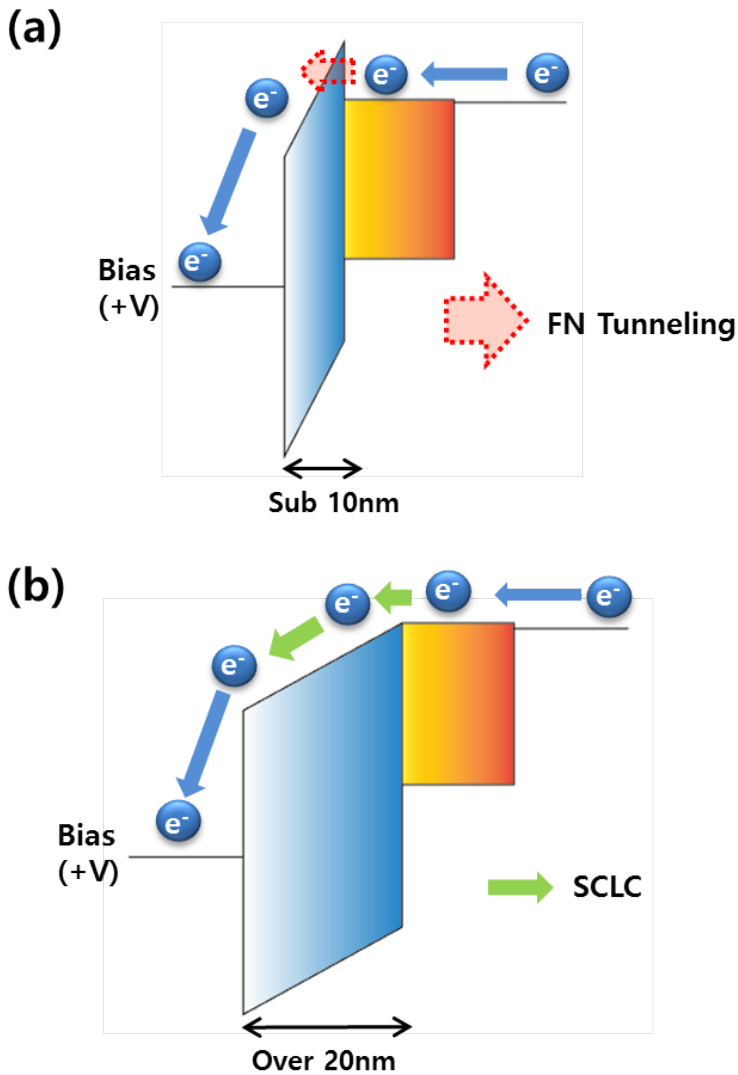

Figure 12. (a) The band diagram of tETO of sub-10nm at the forward bias. It shows the F-N tunneling mechanism. (b) The band diagram of tETO of over-20nm. It shows the SCLC mechanism.

4. Conclusion

In conclusion, MEEM diodes with an ultra-thin film insulator (t_{ETO} = 3 nm) have a strongly enhanced forward current (0.16 A/cm^2) and high rectifying ratio (2×10^7) at low voltages (3 V), enabling them to be used in low power applications. Particularly noteworthy is the shift of the electrical current conduction mechanism in the MEEM diode at a certain t_{ETO}. The electric currents follow the SCLC conduction mechanism when the thickness of the ETO, t_{ETO}, exceeds 20 nm, and follow the quantum tunneling conduction mechanism, F-N tunneling, when the t_{ETO} is 10 nm or less. There is a variation in the barrier height with the t_{ETO} in oxide hetero-interface diodes, or MEEM diodes. The existence of a t_{ETO}^{cr} is verified by showing that the barrier height decreases as the t_{ETO} becomes thicker. In addition, it was shown that the barrier height of the MEEM structure is significantly decreased compared to the MIM structure. This is an indirect indication that the dipole moments are generated at the ETO / EIO interface, and the barrier height variations are caused by these dipoles. As a result, these MEEM diodes with improved electrical current have the potential to be applied to a variety of low power nanotechnology applications such as transparent display devices, transparent micro-electro-mechanical systems, and resistive random-access memory selectors.

References

1. Burroughes, J. H., Bradley, D. D. C., Brown, A. R., Marks, R. N., Mackay, K., Friend, R. H., Burns, P. L. & Holmes, A. B. Light-emitting diodes based on conjugated polymers. *Nature* **347,** 539–541 (1990).

2. Yablonovitch, E., Kapon, E., Gmitter, T. J., Yun, C. P. & Bhat, R. Double heterostructure GaAs/AlGaAs thin film diode lasers on glass substrates. *IEEE Photonics Technol. Lett.* **1,** 41–42 (1989).

3. Hollahan, J. R., Rosler, R. S., Vossen, J. L. & Kern, W. Thin Film Processes. *Acad. New York* (1978).

4. Kudo, A., Yanagi, H., Ueda, K., Hosono, H., Kawazoe, H. & Yano, Y. Fabrication of transparent p–n heterojunction thin film diodes based entirely on oxide semiconductors. *Appl. Phys. Lett.* **75,** 2851–2853 (1999).

5. Chen, C. H., Chang, S.-J., Su, Y.-K., Chi, G.-C., Chi, J.-Y., Chang, C. A., Sheu, J.-K. & Chen, J.-F. GaN metal-semiconductor-metal ultraviolet photodetectors with transparent indium-tin-oxide Schottky contacts. *IEEE Photonics Technol. Lett.* **13,** 848–850 (2001).

6. Zhang, S. & Sin, J. K. O. A novel self-aligned bidirectional MIM diode with transparent junctions for AM-LCD's. *IEEE Electron Device Lett.* **19,** 192–194 (1998).

7. Baco, S., Chik, A. & Yassin, F. M. Study on optical properties of tin oxide thin film at different annealing temperature. *J. Sci. Technol.* **4,** (2012).

8. Janotti, A. & Van de Walle, C. G. Fundamentals of zinc oxide as a semiconductor. *Reports Prog. Phys.* **72,** 126501 (2009).

9. Wang, J. T., Shi, X. L., Liu, W. W., Zhong, X. H., Wang, J. N., Pyrah, L., Sanderson, K. D., Ramsey, P. M., Hirata, M. & Tsuri, K. Influence of preferred orientation on the electrical conductivity of fluorine-doped tin oxide films. *Sci. Rep.* **4,** (2014).

10. Ahmad, H., Kamarudin, S. K., Minggu, L. J. & Kassim, M. Hydrogen from photo-catalytic water splitting process: a review. *Renew. Sustain. Energy Rev.* **43,** 599–610 (2015).

11. Hautier, G., Miglio, A., Ceder, G., Rignanese, G.-M. & Gonze, X. Identification and design principles of low hole effective mass p-type transparent conducting oxides. *Nat. Commun.* **4,** (2013).

12. Lee, H.-Y. & Chern, M.-Y. Optical properties of ITO/ZnO Schottky diode with enhanced UV Photoresponse. *J. Korean Phys. Soc.* **67,** 1804–1808 (2015).

13. Zhang, J., Li, Y., Zhang, B., Wang, H., Xin, Q. & Song, A. Flexible indium-gallium-zinc-oxide Schottky diode operating beyond 2.45 [thinsp] GHz. *Nat. Commun.* **6,** (2015).

14. Lee, E., Lee, J., Kim, J.-H., Lim, K.-H., Byun, J. S., Ko, J., Kim, Y. D., Park, Y. & Kim, Y. S. Direct electron injection into an oxide insulator using a cathode buffer layer. *Nat. Commun.* **6,** (2015).

15. Park, Y., Lee, E., Lee, J., Lim, K.-H. & Kim, Y. S. Unidirectional oxide hetero-interface thin-film diode. *Appl. Phys. Lett.* **107,** 143506 (2015).

16. Lampert, M. A. Simplified theory of space-charge-limited currents in an insulator with traps. *Phys. Rev.* **103,** 1648 (1956).

17. Lenzlinger, M. & Snow, E. H. Fowler-Nordheim tunneling into thermally grown SiO2. *J. Appl. Phys.* **40,** 278–283 (1969).

18. Gusev, E. P., Cartier, E., Buchanan, D. A., Gribelyuk, M., Copel, M., Okorn-Schmidt, H. & D'emic, C. Ultrathin high-K metal oxides on silicon: processing, characterization and integration issues. *Microelectron. Eng.* **59,** 341–349 (2001).

19. Narasimha, K. T., Ge, C., Fabbri, J. D., Clay, W., Tkachenko, B. A., Fokin, A. A., Schreiner, P. R., Dahl, J. E., Carlson, R. M. K. & Shen, Z. X. Ultralow effective work function surfaces using diamondoid monolayers. *Nat. Nanotechnol.* **11,** 267–272 (2016).

20. Cameron, A. C. & Windmeijer, F. A. G. An R-squared measure of goodness of fit for some common nonlinear regression models. *J. Econom.* **77,** 329–342 (1997).

21. Zhao, C., Zhao, C. Z., Taylor, S. & Chalker, P. R. Review on non-volatile memory with high-k dielectrics: flash for generation beyond 32 nm. *Materials (Basel).* **7,** 5117–5145 (2014).

22. Huang, X. D., Liu, L., Xu, J. P. & Lai, P. T. Improved Performance of Yttrium-Doped Al_2O_3 as Inter-Poly Dielectric for Flash-Memory Applications. *IEEE Trans. Device Mater. Reliab.* **11,** 490–494 (2011).

23. Liu, Z. Q., Chim, W. K., Chiam, S. Y., Pan, J. S. & Ng, C. M. An interface dipole predictive model for high-k dielectric/semiconductor heterostructures using the concept of the dipole neutrality point. *J. Mater. Chem.* **22,** 17887–17892 (2012).

24. Yamamoto, Y., Kita, K., Kyuno, K. & Toriumi, A. Study of La-induced flat band voltage shift in metal/HfLaOx/SiO2/Si capacitors. *Jpn. J. Appl. Phys.* **46,** 7251 (2007).

25. Kita, K. & Toriumi, A. Origin of electric dipoles formed at high-k/SiO 2 interface. *Appl. Phys. Lett.* **94,** 132902 (2009)..

26. Helander, M. G., Wang, Z. B., Qiu, J. & Lu, Z. H. Band alignment at metal/organic and metal/oxide/organic interfaces. *Appl. Phys. Lett.* **93,** 412 (2008).

27. Meyer, J., Kröger, M., Hamwi, S., Gnam, F., Riedl, T., Kowalsky, W. & Kahn, A. Charge generation layers comprising transition metal-oxide/organic interfaces: Electronic structure and charge generation mechanism. *Appl. Phys. Lett.* **96,** 93 (2010).

28. Singh-Bhalla, G., Bell, C., Ravichandran, J., Siemons, W., Hikita, Y., Salahuddin, S., Hebard, A. F., Hwang, H. Y. & Ramesh, R. Built-in and induced polarization across LaAlO3/SrTiO3 heterojunctions. *Nat. Phys.* **7,** 80–86 (2011).

29. Ohtomo, A. & Hwang, H. Y. A high-mobility electron gas at the LaAlO3/SrTiO3 heterointerface. *Nature* **427,** 423–426 (2004).

30. Bykhovski, A., Gelmont, B., Shur, M. & Khan, A. Current-voltage characteristics of strained piezoelectric structures. *J. Appl. Phys.* **77,** 1616–1620 (1995).

31. Simon, J., Zhang, Z., Goodman, K., Xing, H., Kosel, T., Fay, P. & Jena, D. Polarization-induced Zener tunnel junctions in wide-band-gap heterostructures. *Phys. Rev. Lett.* **103,** 26801 (2009).

32. Chen, K., Zhu, H., Yi, X., Cheng, S., Li, J., Wang, S., Lu, M., Xu, M., Ma, L. & Lü, L. Role of oxygen defects in inducing the blue photoluminescence of zinc oxide films deposited by magnetron sputtering. *Chinese Opt. Lett.* **13,** 103101 (2015).

33. Özgür, Ü., Alivov, Y. I., Liu, C., Teke, A., Reshchikov, Ma., Doğan, S., Avrutin, V., Cho, S.-J. & Morkoc, H. A comprehensive review of ZnO materials and devices. *J. Appl. Phys.* **98,** 11 (2005).

34. Wang, Z. B., Helander, M. G., Greiner, M. T., Qiu, J. & Lu, Z.-H. Carrier mobility of organic semiconductors based on current-voltage characteristics. *J. Appl. Phys.* **107,** 34506 (2010).

35. Wang, Z. B., Helander, M. G., Greiner, M. T., Qiu, J. & Lu, Z. H. Analysis of charge-injection characteristics at electrode-organic interfaces: Case study of transition-metal oxides. *Phys. Rev. B* **80,** 235325 (2009).

36. Toriumi, Ak. & Nabatame, T. Anomalous VFB Shift in High-k Gate Stacks-Is its Origin at the Top or Bottom Interface?-. *ECS Trans.* **25,** 3–16 (2009).

요약 (국문초록)

신개념의 산화물 적층 구조의 박막 다이오드를 저전압에서 높은 전류 밀도를 갖도록하는 효과적이고 쉬운 방법을 제안한다. 이 다이오드의 전류 특성은 절연체의 두께에 따라 두가지 메커니즘으로 지배된다. 흥미롭게도 이 메커니즘들은 절연체의 특정 임계 두께에서 확연히 구분이 된다. 절연체의 두께가 10nm 이하에서는 공간 전하 제한 전류 (SCLC) 모델과 일치하며 20nm 이상에서는 파울러-노드하임 (F-N) 터널링 특성을 보인다. 심층적인 분석으로 이 현상은 절연체의 두께가 증가함에 따라 절연체-반도체의 계면에서 장벽 높이가 감소하는 특성 때문임을 증명하였으며 또한 이 박막 다이오드의 장벽 높이가 절연체 두께의 조절로 엔지니어링이 가능함을 보여주었다. 따라서 초 박막 절연체를 갖는 산화물 적층 구조의 다이오드는 저전압 구동이 가능하여 저전력의 투명 나노 어플리케이션에 무한한 잠재력을 가지고 있다.

주요어 : 산화물 적층 계면, 박막 다이오드, 장벽 높이, 메커니즘 시프트, 계면 쌍극자

학 번 : 2015-26090